

Yi Zhang, Hui Dong, Hans-Joachim Krause,
Guofeng Zhang, and Xiaoming Xie

SQUID Readout Electronics and Magnetometric Systems for Practical Applications

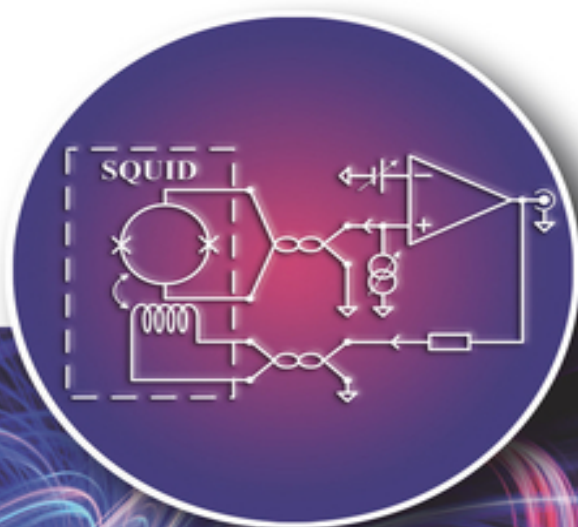


Table of Contents

[Cover](#)

[Preface](#)

[Acknowledgments](#)

[1 Introduction](#)

[1.1 Motivation](#)

[1.2 Contents of the Chapters](#)

[References](#)

[2 Josephson Junctions](#)

[2.1 Josephson Equations](#)

[2.2 RCSJ Model](#)

[References](#)

[3 dc SQUID's \$I\$ - \$V\$ Characteristics and Its Bias Modes](#)

[3.1 SQUID's \$I\$ - \$V\$ Characteristics](#)

[3.2 An Ideal Current Source](#)

[3.3 A Practical Voltage Source](#)

[References](#)

[4 Functions of the SQUID's Readout Electronics](#)

[4.1 Selection of the SQUID's Bias Mode](#)

[4.2 Flux Locked Loop \(FLL\)](#)

[4.3 Suppressing the Noise Contribution from the Preamplifier](#)

[4.4 Two Models of a dc SQUID](#)

[References](#)

[5 Direct Readout Scheme \(DRS\)](#)

[5.1 Introduction](#)

[5.2 Readout Electronics Noise in DRS](#)

[5.3 Chain Rule and Flux Noise Contribution of a Preamplifier](#)

[5.4 Summary of the DRS](#)

[References](#)

[6 SQUID Magnetometric System and SQUID Parameters](#)

[6.1 Field-to-Flux Transformer Circuit \(Converter\)](#)

[6.2 Three Dimensionless Characteristic Parameters, \$\beta_c\$, \$\Gamma\$, and \$\beta_L\$, in SQUID Operation](#)

[References](#)

[7 Flux Modulation Scheme \(FMS\)](#)

[7.1 Mixed Bias Modes](#)

[7.2 Conventional Explanation for the FMS](#)

[7.3 FMS Revisited](#)

[7.4 Conclusion](#)

[References](#)

[8 Flux Feedback Concepts and Parallel Feedback Circuit](#)

[8.1 Flux Feedback Concepts and History](#)

[8.2 SQUID's Apparent Parameters](#)

[8.3 Parallel Feedback Circuit \(PFC\)](#)

[8.4 Quantitative Analyses and Experimental Verification of the PFC in Voltage Bias Mode](#)

[8.5 Main Achievements of PFC Quantitative Analysis](#)

[8.6 Comparison with the Noise Behaviors of Two Preamplifiers](#)

[References](#)

[9 Analyses of the "Series Feedback Coil \(Circuit\)" \(SFC\)](#)

[9.1 SFC in Current Bias Mode](#)

[9.2 The SFC in Voltage Bias Mode](#)

[9.3 Summary of the PFC and SFC](#)

[9.4 Combination of the PFC and SFC \(PSFC\)](#)

[References](#)

[10 Weakly Damped SQUID](#)

[10.1 Basic Consideration of Weakly Damped SQUID](#)

[10.2 SQUID System Noise Measurements with Different \$\beta_c\$ Values](#)

[10.3 Statistics of SQUID Properties](#)

[10.4 Single Chip Readout Electronics \(SCRE\)](#)

[10.5 Suggestions for the DRS](#)

[References](#)

[11 Two-Stage and Double Relaxation Oscillation Readout Schemes](#)

[11.1 Two-Stage Scheme](#)

[11.2 ROS and D-ROS](#)

[11.3 Some Comments on D-ROS and Two-Stage Scheme](#)

[References](#)

[12 Radio-Frequency \(rf\) SQUID](#)

[12.1 Fundamentals of an rf SQUID](#)

[12.2 Conventional rf SQUID System](#)

[12.3 Introduction to Modern rf SQUID Systems](#)

[12.4 Further Developments of the rf SQUID Magnetometer System](#)

[12.5 Multichannel High-T_c rf SQUID Gradiometer](#)

[12.6 Comparison of rf SQUID Readout with dc SQUID Readout](#)

[12.7 Summary and Outlook](#)

[References](#)

[Index](#)

[End User License Agreement](#)

List of Tables

Chapter 6

[Table 6.1 Parameters of LTS SQUID magnetometers with \$A_p\$ of \$5 \times 5 \text{ mm}^2\$.](#)

[Table 6.2 Parameters of LTS SQUID magnetometers with \$A_p\$ of \$10 \times 10 \text{ mm}^2\$.](#)

[Table 6.3 SQUID parameters measured by the DRS.](#)

Chapter 7

[Table 7.1 Comparison of schematic diagrams of a DRS and the FMS.^{a\)}](#)

[Table 7.2 Measured \$\Delta i\$ and \$V_{RS}\$.](#)

Chapter 8

[Table 8.1 Feedback circuits in the two bias modes.](#)

[Table 8.2 Measured parameters of SQUIDs with and without PFC.](#)

[Table 8.3 Noise data and analysis for SQUIDs with and without the PFC.](#)

Chapter 9

[Table 9.1 Parameters of the SQUID magnetometer.](#)

[Table 9.2 Summary of PFC and SFC at working point W.](#)

[Table 9.3 Parameters of PSBC in experiment II.](#)

Chapter 10

[Table 10.1 Slew rates at different frequencies.](#)

Chapter 12

[Table 12.1 SQUID parameters and the measured system noise with \$f_L \approx 150\$ MHz.](#)

[Table 12.2 Characteristics of the tank circuit with an inductive coupling and...](#)

[Table 12.3 Parameters of different labyrinth resonators.](#)

[Table 12.4 SQUID loop size and corresponding \$\partial B/\partial \Phi\$.](#)

[Table 12.5 Voltage-to-flux coefficient \(\$V/\Phi_0\$ \) of FLL measured with different ...](#)

[Table 12.6 Bandwidth in kHz, measured with a SQUID in FLL with the integrator...](#)

List of Illustrations

Chapter 2

[Figure 2.1 A Josephson element \$J\$, a capacitance \$C\$, and a resistance \$R_J\$ are c...](#)

[Figure 2.2 \$I\$ - \$V\$ characteristics for different \$\beta_c\$ values: \(a\) \$\beta...\$](#)

[Figure 2.3 Schematic illustrations of the \$I\$ - \$V\$ characteristics with dif...](#)

[Figure 2.4 \$I\$ - \$V\$ characteristics of two SIS junctions in the RCSJ model with d...](#)

Chapter 3

[Figure 3.1 Schematic diagram of a four-pole \(terminal\) measuring method. Her...](#)

[Figure 3.2 \$I\$ - \$V\$ characteristics of a resistor \(a\) and a diode \(b\), wher...](#)

[Figure 3.3 The SQUID's \$I\$ - \$V\$ characteristics are divided into three regi...](#)

[Figure 3.4 Principle circuits of current bias mode \(a\) and voltage bias mode...](#)

[Figure 3.5 Practical circuit of the current bias mode for measuring SQUID dy...](#)

[Figure 3.6 Two possible concepts for realizing voltage bias mode. \(a\) A curr...](#)

Chapter 4

[Figure 4.1 The \$I\$ - \$V\$ characteristics are the SQUID's essence, while \$V\(\Phi\)\$...](#)

[Figure 4.2 \(a\) A linearly changing flux \$\Phi\(t\)\$ with time and the expected outp...](#)

[Figure 4.3 In dc SQUID magnetometry, the "head stage" consists of at least t...](#)

[Figure 4.4 A fundamental circuit of a SQUID's readout electronics with an FL...](#)

[Figure 4.5 Schematic diagram of working point selection from \$V\(\Phi\)\$ in a perio...](#)

[Figure 4.6 \(a\) The dynamic balancing process of the working point when a tra...](#)

[Figure 4.7 For readout electronics, a dc SQUID can be described with either ...](#)

Chapter 5

[Figure 5.1 The test circuit of an op-amp functioning as a voltage amplifier ...](#)

[Figure 5.2 The measured noise spectra of \$I_n\$ \(left vertical axis\) and \$V_n\$ \(rig...](#)

[Figure 5.3 Test circuit of a PCBT as a voltage amplifier with \$G = 1000\$ for c...](#)

[Figure 5.4 The measured noise spectra of \$I_n\$ \(left vertical axis\) and \$V_n\$ \(rig...](#)

[Figure 5.5 The voltage noise \$\delta V_e\$ of an AD797 acting as a voltage preamp...](#)

[Figure 5.6 The total voltage noise \$\delta V_e\$ of a PCBT acting as a voltage pr...](#)

[Figure 5.7 \(a\) Schematic diagram showing the test circuit, where the same pr...](#)

[Figure 5.8 Noise measurements of a strongly damped SQUID with \$\beta_c \approx 0.3\$...](#)

Chapter 6

[Figure 6.1 \(a\) Schematic "head stage" of a SQUID magnetometric system, consi...](#)

[Figure 6.2 Measured \$V\(\Phi\)\$ curves of current-biased SQUIDs with \$L_s \approx 350\$ pH: \(...](#)

[Figure 6.3 Three simulated \$I\$ - \$V\$ characteristics of a symmetric SQUID wi...](#)

[Figure 6.4 Geometrical images of three typical \$\beta_L\$ values, \$\beta_L \approx 0\$ \(...](#)

[Figure 6.5 The tendencies of the three electrically readable SQUID values wi...](#)

Chapter 7

[Figure 7.1 The input circuit \(head stage\) is a SQUID shunted by an element \$Z\$](#)

Figure 7.2 A schematic diagram of the FMS. The SQUID is biased by a constant...

Figure 7.3 (a) A linearly changing flux $\Phi(t)$ results in a periodic SQUID's V

Figure 7.4 $\Phi(t)$, $V_s(\Phi)$, and $V_{M1}(t)$ in a modulation period for the case of a ...

Figure 7.5 The left column shows the positions of the modulation points, W_M ...

Figure 7.6 Working principle diagram of FMS demonstrated with $\Phi(t)$, $V_s(\Phi)$, a...

Figure 7.7 If $\Delta\Phi < \Phi_0/4$ (see point 1) or $\Delta\Phi > \Phi_0/4$ (see point 2) in $T_M/2$, th...

Figure 7.8 The frequency spectrum of V_{M1} . The peaks present the Fourier comp...

Figure 7.9 SQUID input circuit of FMS with a step-up transformer and preampl...

Figure 7.10 The simplified input circuit by replacing Z_s with a variable res...

Figure 7.11 Test circuit for determining V_{out} and Δi of the SQUID (SQ1) with...

Figure 7.12 Measured SQUID's I - V characteristics at $\Phi = n\Phi_0$ and $\Phi = (n$

Figure 7.13 The test circuit simulates the SQUID's input circuit for measuri...

Figure 7.14 Complex transfer characteristics measured by a frequency respons...

Figure 7.15 A square wave signal with dashed line (right axis) passing throu...

[Figure 7.16 The \$V\(\Phi\)\$ characteristics of a SQUID with a loop inductance \$L_s = \dots\$](#)

Chapter 8

[Figure 8.1 The SQUID's "head stage" with the PFC and SFC. Here, the PFC is a...](#)

[Figure 8.2 Four schematic diagrams of a modified DRS at the "head stage" wit...](#)

[Figure 8.3 Schematic diagram of a circuit containing a resistor \$R\$ and two ba...](#)

[Figure 8.4 In current bias mode, the equivalent circuit of a SQUID shunted b...](#)

[Figure 8.5 Two measured SQUID's \$I-V\$ characteristics: the original one with t...](#)

[Figure 8.6 The SQUID's \$V\(\Phi\)\$ characteristics without \(step \(i\)\) and with the ...](#)

[Figure 8.7 The experimentally recorded data: the dashed lines represent the ...](#)

[Figure 8.8 The \$V\(\Phi\)\$ characteristics with the PFC \(APF\) are schematically sho...](#)

[Figure 8.9 \(a\) A SQUID shunted by a PFC \(NC scheme\) connects to the invertin...](#)

[Figure 8.10 The equivalent circuit of \$V_n\$ of an op-amp \(preamplifier\) in volt...](#)

[Figure 8.11 Schematic of the \$I\(\Phi\)\$ characteristics in the NC scheme, where th...](#)

[Figure 8.12 There are two circuits for the noise analyses: \(a\) is equivalent...](#)

[Figure 8.13 The \$I-V\$ characteristics \(photo\) measured near \$\Phi = \(2n + 1\)\Phi_0/4\$ w...](#)

[Figure 8.14 Dependence of numerically calculated flux noise contributions, \$\delta\Phi_{\text{PFC}}\$...](#)

[Figure 8.15 Dependence of \$\delta\Phi_{\text{PFC}}\$ on \$\Delta\$ at \$r = 1\$ \(a\), \$r = 3\$ \(b\), and \$r = 5\$ \(c\) ...](#)

[Figure 8.16 Numerically calculated \$\delta\Phi_{\text{PFC}}\(\Delta\)\$ and \$\(R_{\text{d}}\)_{\text{PFC}}\(\Delta\)\$. The solid \(black...](#)

[Figure 8.17 Flux noise spectra of SQUID #2 measured \(I\) with the PFC in the ...](#)

[Figure 8.18 Current noise spectra of the employed PCBT preamplifier: curves ...](#)

[Figure 8.19 The measured spectra \$\delta\Phi_{\text{sys}}\$: curves I \(PFC\) and II \(two-stage sch...](#)

[Figure 8.20 The \$R_{\text{p}}\$ of the PFC is replaced by an FET, where \$V_{\text{gs}}\$ controls the ...](#)

[Figure 8.21 The equivalent circuit of design \(2\) with selectable \$M_{\text{p}}\$ and \$R_{\text{p}}\$, ...](#)

[Figure 8.22 An example of design \(2\): a niobium SQUID magnetometer layout wi...](#)

[Figure 8.23 Illustrations plotting the current noise \$\delta I\$ spectra \(right ordin...](#)

Chapter 9

[Figure 9.1 The arrangement of the SFC, where the coil \$L_{\text{se}}\$ and the SQUID are ...](#)

[Figure 9.2 \(a\) The measured \$V\(\Phi\)\$ characteristics are unchanged with and with...](#)

[Figure 9.3 Measured system noise \$\delta\Phi_{\text{sys}}\$ without \(I\) and with the SFC \(II\) and...](#)

[Figure 9.4 The equivalent circuit of a voltage-biased SQUID with SFC.](#)

[Figure 9.5 In voltage bias mode, the \$I\(\Phi\)\$ characteristics without \(dotted cu...](#)

[Figure 9.6 Hysteresis appears in the measured \$I\(\Phi\)\$ characteristics, as \$M_{se} \times \dots\$](#)

[Figure 9.7 The SQUID with the PSFC in voltage bias mode, where both the \$L_{se} \dots\$](#)

[Figure 9.8 Four equivalent circuits of the PSFC under the independence condi...](#)

[Figure 9.9 Working point \$W_2\$ is set on the steep slope of the asymmetric \$I\(\Phi\) \dots\$](#)

[Figure 9.10 The flux noise spectrum and the corresponding field sensitivity ...](#)

[Figure 9.11 The measured \$I\(\Phi\)\$ characteristics for three different values of](#)

[Figure 9.12 Comparison of the system flux and field noise spectra measured w...](#)

[Figure 9.13 Plots of \$I\(\Phi\)_{PSFC}\$ and \$\(\partial I / \partial \Phi\)_{PSFC}\$ vs. \$\Phi / \Phi_0\$ at \$M_{se} = 0.09\$ nH. The...](#)

Chapter 10

[Figure 10.1 System noise \$\delta\Phi_{sys}\$ measurements \(right ordinate gives the field ...](#)

[Figure 10.2 Noise characteristics of the SQUID with \$\beta_c \approx 3.5\$. The inset...](#)

[Figure 10.3 Statistical data of \$I_{swing}\$ \(a\) and \$R_d\$ \(b\) of 101 SQUIDs as a fun...](#)

[Figure 10.4 Statistical characterization of 53 SQUIDs with nominal \$R_J = 30 \Omega\$...](#)

[Figure 10.5 \(a\) \$\delta B_{\text{sys}}\$ classification of the 53 voltage-biased SQUID magnetom...](#)

[Figure 10.6 Schematic diagram of SCRE with a current-biased SQUID. The AD797...](#)

[Figure 10.7 Flux noise \(left scale\) and field noise \(right scale\) measured i...](#)

[Figure 10.8 The equivalent electronic circuits of SCRE in FLL \(shown in Figu...](#)

[Figure 10.9 MCG signal of an adult male subject recorded in an MSR.](#)

[Figure 10.10 Schematic real-time TEM signal \(a\) and its enlargement \(b\) reco...](#)

Chapter 11

[Figure 11.1 In principle, the voltage-biased circuit needs an ammeter "A" to...](#)

[Figure 11.2 Different concepts of FLL operation in the two-stage scheme: two...](#)

[Figure 11.3 Suggestion of a practical SQUID magnetometric system with a two-...](#)

[Figure 11.4 \$V\(\Phi\)\$ characteristics at \$V_{\text{out}}\$, where the real characteristics of ...](#)

[Figure 11.5 Hysteretic \$I\$ - \$V\$ characteristics of an unshunted SQUID. The...](#)

[Figure 11.6 The equivalent circuit of ROS. The virtual voltmeter and ammeter...](#)

[Figure 11.7 Simulated \$I_1\$ \(upper\) and \$V_s\$ \(lower\) of an ROS in the time domain...](#)

[Figure 11.8 Schematic arrangement of D-ROS where the output voltage drops ac...](#)

Chapter 12

[Figure 12.1 The magnetic flux relationship inside and outside the SQUID loop...](#)

[Figure 12.2 \(a\) Readout principle of an rf SQUID: the rf SQUID is coupled to...](#)

[Figure 12.3 Illustration of the rf SQUID behavior in dissipative mode \(\$\beta...\$](#)

[Figure 12.4 rf SQUID behavior in dispersive mode \(\$\beta_e \ll 1\$ \): \(a\) the rf S...](#)

[Figure 12.5 At \$\beta_e \approx 1\$, both effects on the tank circuit caused by the r...](#)

[Figure 12.6 Block diagram of the 30 MHz version of rf SQUID readout electron...](#)

[Figure 12.7 Schematic illustration of a mixture of technologies, i.e. a mode...](#)

[Figure 12.8 The improved parts of rf SQUID readout electronics that are diff...](#)

[Figure 12.9 Modified conventional LC tank circuit with inductive coupling pl...](#)

[Figure 12.10 Schematics of the first planar tank circuit for rf SQUID operat...](#)

[Figure 12.11 \(a\) Schematic diagram of the \$\lambda\$ resonator integrated with a...](#)

[Figure 12.12 \(A\) Schematic of three flux concentrator/coplanar resonator lay...](#)

[Figure 12.13 \(a\) In the rf SQUID tank circuit, the schematic rf EM field dis...](#)

[Figure 12.14 \(a\) Two arrangements of a practical encapsulated SQUID magnetom...](#)

[Figure 12.15 Noise spectrum of a YBCO rf SQUID magnetometer with a SrTiO₃ di...](#)

[Figure 12.16 \(a\) Measured \$V_{\text{rf}}\(\Phi\)\$ characteristics of an rf SQUID coupled with...](#)

[Figure 12.17 Typical \$V_{\text{rf}}\(\Phi\)\$ characteristics of rf SQUIDs in the planar labyr...](#)

[Figure 12.18 Schematic arrangements of two cylindrical coils, \$L_{\text{in}}\$ and \$L_{\text{T, in}}\$...](#)

[Figure 12.19 Layout of the rf SQUID magnetometer with an rf labyrinth resona...](#)

[Figure 12.20 System flux noise \$\delta\Phi_{\text{sys}}\$ of a high- \$T_{\text{c}}\$ rf SQUID magnetometer with...](#)

[Figure 12.21 Schematic of the modern rf SQUID readout electronics.](#)

[Figure 12.22 \(a\) Top: amplification as a function of frequency; bottom: rf p...](#)

[Figure 12.23 \(a\) SQUID signal as a function of attenuator voltage \(which tra...](#)

[Figure 12.24 \(a\) Schematic sketch of a four-channel electronic gradiometer, ...](#)

[Figure 12.25 Four-channel gradient fMCG signals from a fetus at a gestationa...](#)

[Figure 12.26 Averaged fMCG data with a 75 seconds duration.](#)

[Figure 12.27 The transfer characteristics of the tank circuit in SQUID opera...](#)

Figure 12.28 Reflected power and phase as a function of pumping frequency fo...

SQUID Readout Electronics and Magnetometric Systems for Practical Applications

Yi Zhang

Hui Dong

Hans-Joachim Krause

Guofeng Zhang

Xiaoming Xie

Authors

Prof. Dr. Yi Zhang

Forschungszentrum Jülich (Retired)
Institute of Biological Information Processing
Wilhelm-Johnen-Straße
52428 Jülich
Germany

Prof. Dr. Hui Dong

Shanghai Institute of Microsystem and Information Technology
865 Changning Road
200050 Shanghai
China

Prof. Dr. Hans-Joachim Krause

Forschungszentrum Jülich
Institute of Biological Information Processing
Wilhelm-Johnen-Straße
52428 Jülich
Germany

Dr. Guofeng Zhang

Shanghai Institute of Microsystem and Information Technology
865 Changning Road
200050 Shanghai
China

Prof. Dr. Xiaoming Xie

Shanghai Institute of Microsystem and Information Technology
ShanghaiTech University
University of Chinese Academy of Sciences
865 Changning Road
200050 Shanghai
China

All books published by **Wiley-VCH** are carefully produced. Nevertheless, authors, editors, and publisher do not warrant the information contained in these books, including this book, to be free of errors. Readers are advised to

keep in mind that statements, data, illustrations, procedural details or other items may inadvertently be inaccurate.

Library of Congress Card No.: applied for

British Library Cataloguing-in-Publication Data

A catalogue record for this book is available from the British Library.

Bibliographic information published by the Deutsche Nationalbibliothek

The Deutsche Nationalbibliothek lists this publication in the Deutsche Nationalbibliografie; detailed bibliographic data are available on the Internet at <<http://dnb.d-nb.de>>.

© 2020 Wiley-VCH Verlag GmbH & Co. KGaA, Boschstr. 12, 69469 Weinheim, Germany

All rights reserved (including those of translation into other languages). No part of this book may be reproduced in any form – by photoprinting, microfilm, or any other means – nor transmitted or translated into a machine language without written permission from the publishers. Registered names, trademarks, etc. used in this book, even when not specifically marked as such, are not to be considered unprotected by law.

Print ISBN: 978-3-527-34488-8

ePDF ISBN: 978-3-527-81650-7

ePub ISBN: 978-3-527-81652-1

oBook ISBN: 978-3-527-81651-4

Cover Design Adam-Design,

Weinheim, Germany

Preface

Time flies! Thirteen years ago, as a research professor at Shanghai Institute of Microsystem and Information Technology (SIMIT), Chinese Academy of Sciences (known as Shanghai Institute of Metallurgy by that time), I was charged with a challenging mission, to start a team on superconducting electronics research. From the institute, it was a quite straightforward decision, as the whole institute had been gradually shifting from materials science research toward electronics and systems. And for myself, it was not so easy to start something new at the age over 40, with a strong background on superconducting materials, some basic knowledge on electronics but little on superconducting electronics. Just when I was wondering how to do that, Prof. P.H. Wu, a member of Chinese Academy of Sciences, a famous professor in the field of superconducting electronics in China, who had worked at Research Center Julich (FZJ) Germany, recommended me Dr. Yi Zhang, a reputable German scientist at FZJ, born in Shanghai, acknowledged globally for his excellent research on the development of high T_c radio-frequency superconducting quantum interference devices (high temperature superconducting [HTS] rf SQUIDs), their readout electronics and systems. I contacted FZJ without hesitation, inviting Yi to act as a consultant to our first project on SQUID-based Magnetocardiography (MCG) system. This request letter opened the door of cooperation between SIMIT and FZJ. To date, our cooperation has developed from a project collaboration between two professors to the establishment of two joint research laboratories and further to a virtual joint research institute. The cooperation also has been extended from

superconductivity to topological insulators and quantum computing.

After some formal procedures, I got the approval of my request letter from Prof. Dr. Joachim Treusch, the former chairman of the board of directors of FZJ, Prof. Dr. Sebastian Schmidt, a current member of the board of directors of FZJ, and Prof. Dr. Andreas Offenhäusser, director of IBN2 (Institute of Bio and Nanoscience, now Institute of Biological Information Processing), which Yi belonged to. Besides the support from the top management, the involvement of Prof. Dr. Hans-Joachim Krause, team leader of magnetic sensors in IBN2, was another important step for our successful cooperation.

Our joint research on dc SQUID started from the development of asymmetrical SQUID characteristics, in an attempt to simplify SQUID readout and system design. The adventure was full of excitement and frustration. Early in the morning, we sat together, planning the work of the day, late in the evening, we summarized our results from the notes we made during the day, sometimes exciting progress, sometimes frustrating results, and sometimes confusing results which we could not describe easily. I still remember how excited we were when we first observed the asymmetrical flux-current characteristics of a SQUID on the oscilloscope, and I remembered as well how much we were frustrated when we learnt that the desired asymmetrical characteristics did not lead to the lower noise we had sought for so long. The notes piled up day after day, getting thicker and thicker, we called them "Rabe's Diary." After numerous discussions back and forth, we succeeded in interpreting our results, which led to our first joint publication and our joint patent on the so-called "SQUID Bootstrap Circuit," and to many other joint publications in the following 10 more years.

The SQUID research was more difficult than we first thought because setting up SQUID systems for applications requires the involvement of people from several different disciplines. A complete understanding for SQUID systems needs comprehensive knowledge not only in quantum physics and low-temperature physics but also in material science and electronics engineering. In fact, electrical or electronics engineers are always needed for system development. Therefore, it is very important to establish a common language that is easily accessible for all people. That was how we got the idea to write this book.

Yi Zhang contributed most to writing of this book, with his experience in SQUID research for 34 years, including more than 10 years of joint research with SIMIT. We have aimed to write this book in a way that is easily understandable for engineers and students, in order to overcome the formidable barrier of “quantum” physics. In this book, e.g. dc SQUIDs are simply treated as resistor-like elements, which are modulated by the magnetic flux. We hope that this book will be appreciated by all people interested in developing and working with SQUIDs and SQUID systems. By inviting engineers into the SQUID “family,” we will have a better chance to transform SQUID from a laboratory toy to an enabling technology that will eventually shape our life.

This book is largely a documentation of the joint achievements accomplished in the cooperation between SIMIT and FZJ in the field of superconducting electronics. We believe that the ongoing collaboration between the two parties will continue to grow, and the cooperation will bring more achievements not only in the field of superconducting electronics but also in other fields in the future.

November 2019.

Acknowledgments

It is our pleasure to acknowledge the generous assistance that has been offered throughout the preparation of this book. Without such help, our task would not have been possible. We owe a special debt of gratitude to all the colleagues from China and Germany who have contributed to the works mentioned in this book. Special thanks to Dr. M. Mück for your constructive comments on [Chapter 6](#). Very special thanks to Dr. H. Soltner for the English language reading. We finally express our heartfelt gratitude to Wiley.

1

Introduction

1.1 Motivation

Superconducting QUantum Interference Devices (SQUIDs) are well known because they are the most sensitive sensors for measuring magnetic flux. In magnetometry, a SQUID with a field-to-flux transformer circuit (converter) construct is a magnetometer with high field sensitivity in the range of fT/\sqrt{Hz} (one millionth of the earth's magnetic field). Therefore, the study of SQUID systems has never stopped.

Many books and reviews have elaborated on the SQUID principle and SQUID magnetometric systems as well as SQUID applications, e.g. "Superconductor Applications: SQUIDs and Machines" edited by B. B. Schwartz and S. Foner [1], "Physics and Applications of the Josephson Effect" edited by A. Barone and G. Paterno [2], and the NATO proceedings "SQUID Sensors: Fundamentals, Fabrication and Applications" edited by H. Weinstock [3]. In particular, "The SQUID Handbook," edited in 2004 by John Clarke and Alex I. Braginski comprehensively summarizes SQUID's theory and practice since SQUIDs have been discovered [4]. Hence, this book has become the new "bible" for researchers in the field. Furthermore, the review of "SQUID Magnetometers for Low-Frequency Applications" by Tapani Ryhänen et al. presented a novel formulation for SQUID operation and SQUID magnetometers for low-frequency applications, taking into account the coupling circuits and electronics [5].

Structurally, a direct current (dc) SQUID is a superconducting ring interrupted with two Josephson

junctions. Predicatively, SQUIDs have very rich physical meanings, e.g. the Aharonov-Bohm effect, flux quantization, Meissner effect, Bardeen-Cooper-Schrieffer (BCS) theory, and the Josephson tunnel effect. However, starting from the view of electronic circuits, our first question is on what a dc SQUID is. In magnetometry, a dc SQUID should be regarded as a resistor-like element where its dynamic resistance is modulated by the flux Φ threading the SQUID's loop. In the readout technique, the dynamic resistance of the SQUID, $R_d(\Phi) = \partial V/\partial I$, i.e. the derivative of the voltage with respect to current, is the fundamental readout quantity, which is embodied in the current-voltage (I - V) characteristics of the SQUID. Here, the changing I - V characteristics are limited by two curves at the integer (upper limit) and half-integer (lower limit) of the flux quantum Φ_0 , which reflect the quantity of magnetic flux in the SQUID loop. There is already abundant "know-how" to read out a resistor R . For example, one can measure a voltage V across R with a constant current flowing through R or measure a current I through R when a constant voltage V is connected to R in parallel. A dc SQUID can either be operated at constant current by measuring the voltage across it (called current bias mode) or at constant voltage by measuring the current through it (called voltage bias mode). In either bias mode, only the SQUID's $V(\Phi)$ or $I(\Phi)$ characteristics emerge. Similar to the change in I - V characteristics with the flux, $V(\Phi)$ and $I(\Phi)$ are also modulated by Φ . In brief, the essence of all three SQUID characteristics is recording the SQUID's dynamic resistance changes, $R_d(\Phi)$.

Generally, a SQUID system consists of the SQUID sensor and its readout electronics. The small SQUID signal leads to difficulty in reading out the SQUID's signal without additional noise contributions from the readout technique. Conventionally, one hopes to suppress such noise

contribution below the intrinsic SQUID noise $\delta\Phi_s$. In other words, the measured system noise almost reaches $\delta\Phi_s$.

The main noise source in readout electronics is the preamplifier, which possesses two independent noise sources: the voltage noise V_n and the current noise I_n . Both of these noise sources are innate to the amplifier chip and cannot be changed. In order to compare these two noise contributions in a SQUID system, both types of electronic noise should be translated into a flux noise, $\delta\Phi_e$, in units of $\Phi_0/\sqrt{\text{Hz}}$ with SQUID's transfer coefficient of $\partial V/\partial\Phi$ or $\partial I/\partial\Phi$. In fact, the original SQUID parameters including the transfer coefficients are also innate to the particular SQUID and cannot be changed. However, the SQUID's apparent parameters at the input terminal of the preamplifier can be modified. Over the past half century, people have developed different readout schemes, where the electronic noise $\delta\Phi_e$ is suppressed by increasing the apparent transfer coefficients once a preamplifier is selected. Indeed, the modification of the apparent parameters is the main thread running through the book. Here, we will change the perspective to discuss the optimization of the SQUID system noise, i.e. how to match the SQUID parameters with the readout electronics.

According to the type of superconducting material used, SQUIDs can be divided into two groups: the low-temperature superconducting (LTS) SQUID, also called low- T_c SQUID, usually operated at 4.2 K (liquid helium temperature); and the high-temperature superconducting (HTS) SQUID, also called high- T_c SQUID, usually operated at 77 K (the liquid nitrogen temperature). The LTS material is typically niobium and HTS material is yttrium barium copper oxide ($\text{YB}_2\text{Cu}_3\text{O}_{7-x}$).

However, according to the working principles, the dc SQUID mentioned above is completely different from the radio frequency (rf) SQUID, which is a superconducting ring interrupted with only one junction. To read the signal from an rf SQUID, it is inductively coupled to an rf tank circuit, which connects to the readout electronics.

In this book, LTS (low- T_c) dc SQUID and HTS (high- T_c) rf SQUID systems, which are often used in magnetometry, will be highlighted. We will share our experiences and lessons, mostly from our own works, with readers, college students, and graduates in physics and engineering who have an interest in SQUID techniques, e.g. how to set up a simple SQUID system for themselves.

1.2 Contents of the Chapters

The book is organized into 12 chapters, where most of the content (from [Chapters 2-11](#)) is about the dc SQUIDs, and only the last chapter is related to rf SQUIDs. However, the dc SQUID bias reversal scheme [[6](#)], the $1/f$ noise study [[7,8](#)], and the special readout scheme for the nano-SQUID [[9,10](#)] are not included.

[Chapter 1](#): This chapter is devoted to our motivation above and the subsequent chapter contents - why did we write this book, and what is it about?

[Chapter 2](#): Because the Josephson junction (JJ) is the key element of SQUIDs, Josephson's equations should be first introduced. Then, JJs are analyzed with the resistively and capacitively shunted junction (RCSJ) model, thus introducing two important parameters: the Stewart-McCumber parameter β_c and the thermal rounding parameter Γ . To observe the features of JJs, one often uses the I - V characteristics, where the hysteresis behavior depends on the values of both β_c and Γ . Actually, the I - V

characteristics describe the changing dynamic resistances R_d of the JJ, i.e. $R_d = \partial V / \partial I$. It was experimentally verified that the value of R_d depends not only on the junction shunt resistor R_j but also on the junction critical current I_c .

Generally, JJs without hysteresis are suitable for SQUID operation. In fact, one habitually transforms the parameters β_c and Γ of the JJ into SQUID operation.

[Chapter 3](#): For readout electronics, the dc SQUID is regarded as dynamic resistance $R_d(\Phi)$ modulated by the flux threading into the SQUID loop. The SQUID's I - V characteristics can be divided into three regions, and the SQUID is operated in the flux-modulated region (II). In fact, the behavior of $R_d(\Phi)$ is embodied in a SQUID's I - V characteristics. To measure a resistance R_d , one can impress a known current (current bias) into a SQUID and observe the voltage across the SQUID's dynamic resistance R_d . Alternatively, one can apply a constant voltage to the SQUID (voltage bias) and measure the current passing through R_d . Owing to the small $R_d \approx 10 \Omega$ of the SQUID, an ideal current bias mode for SQUID operation can easily be realized. In contrast, an ideal voltage bias mode can hardly be achieved, as will be shown in the course of the chapter.

[Chapter 4](#): Almost all SQUID readout electronics developed over the past half century have a common feature: they establish a so-called flux-locked loop (FLL) to realize linearization of the output voltage $V_{\text{out}}(\Phi)$ of the readout electronics; i.e. V_{out} is proportional to the flux change Φ . In this chapter, the principle and realization of the FLL are explained. It is a nulling method where a compensation flux always follows the measured flux, thus resulting in a total flux change of zero in the SQUID loop. In the FLL, the concept of the working point W comes up, and the “locked” and “unlocked” cases are discussed. In the FLL, a small

flux change $\Delta\Phi$ near the working point W appears transiently, and a counter flux $-\Delta\Phi$ immediately compensates it so that the SQUID is continuously operated at a constant flux state. Therefore, the SQUID's $R_d(\Phi)$ near W can be expressed as $R_d(\Phi) = R_d + \Delta R_d$, where R_d is considered a fixed resistance and ΔR_d is a minor change with flux. According to the SQUID's bias modes, ΔR_d is translated into the readout quantity ΔV (or ΔI). For example, in practice, a current-biased SQUID can be regarded as a voltage source, $\Delta V = \Delta\Phi \times (\partial V/\partial\Phi)$, connecting to the fixed R_d in series (which seems to be the internal resistance of the voltage source), where $(\partial V/\partial\Phi)$ is the SQUID's flux-to-voltage transfer coefficient at the working point W . The description of the SQUID by means of a differential dynamic resistance is a new model concept.

[Chapter 5](#): In the case of a direct readout scheme (DRS) where the SQUID directly connects to a preamplifier, the electronics noise $\delta\Phi_e$ is usually much larger than the SQUID intrinsic noise $\delta\Phi_s$. Two types of preamplifiers, commercial op-amps (e.g. AD797 from Analog Devices Inc. or LT1028 from Linear Technology Corp.) and parallel-connected bipolar pair transistors (PCBTs) (e.g. $3 \times$ SSM2210 or $3 \times$ SSM2220 from Analog Devices Inc.), are the most commonly used. Here, the noise characteristics, V_n and I_n , of these two types of preamplifiers are measured separately. Nevertheless, a DRS exhibits several advantages; e.g. the SQUID's original parameters can be directly determined, and the noise contributions from both sides, $\delta\Phi_e$ and $\delta\Phi_s$, can be separately analyzed. Especially, the SQUID's transfer coefficient $\partial V/\partial\Phi$ ($\partial I/\partial\Phi$) at the working point W plays two important roles: (i) it bridges different kinds of noise sources, thus unifying all noise in units of $\Phi_0/\sqrt{\text{Hz}}$, as the SQUID is a flux sensor; and (ii) a

large transfer coefficient is beneficial for reducing $\delta\Phi_e$. In fact, it was experimentally confirmed that the noise contribution of $\delta\Phi_e$ does not depend on the SQUID's bias modes. Furthermore, for strongly damped SQUIDs, $\delta\Phi_e$ in DRS dominates the system noise $\delta\Phi_{\text{sys}}$.

[Chapter 6](#): In a SQUID magnetometric system, one strives for a high magnetic field sensitivity δB_{sys} , which involves two aspects: a field-to-flux transformer circuit (converter) and an ordinary SQUID system with an FLL. The former converts a magnetic field signal B into a flux Φ threading the SQUID loop, while the latter reads out the picked-up Φ . In [Section 6.1](#), the requirements of the converter are discussed. In [Section 6.2](#), we show that the SQUID system is characterized by three dimensionless parameters, β_c , Γ , and β_L . Note that the definitions of β_c and Γ for only a single JJ are given in [Chapter 2](#). During SQUID operation, both parameters must be given a new connotation. Four SQUIDs with different β_c values were characterized. Here, a reasonable interpretation of the observed absence of hysteresis in the SQUID's I - V characteristics at high β_c is given. For SQUID operation, the dimensionless parameter β_L particularly describes the modulation depth of the SQUID. Importantly, $\beta_L \approx 1$ imposes a design condition on the product $L_s I_c$ - namely, all electrically readable values of SQUID parameters increase with increase in the SQUID's nominal β_c .

[Chapter 7](#): The flux modulation scheme (FMS) was first introduced to the SQUID readout in 1968 and quickly became the standard readout technique for current-biased SQUIDs. To date, FMS electronics have been the most extensively used. The basic idea of the FMS is to perform an up-conversion of the SQUID's voltage swing at the input terminal of the preamplifier with a step-up transformer,